Desalination and Water Treatment
www.deswater.com

doi: 10.5004/dwt.2022.28346

255 (2022) 236–241
April

Superior photodegradation activity of MoS_2/TiO_2 nanofibers for phenol under visible light irradiation

Engy A. Nada[a], Heba H. El-Maghrabi[b], Hager R. Ali[c], Saad Abd El-Wahab[a], Dina Y. Sabry[a], Yasser M. Moustafa[c], Amr A. Nada[c,*]

[a]*Chemistry Department, Faculty of Science, Ain shams University, Cairo, Egypt, Tel. +201090298986; email: engyahmednada@gmail.com (E.A. Nada), Tel. +201001426029; email: saadabdelwahab@sci.asu.edu.eg (S.A. El-Wahab), Tel. +201123687707; email: d.y_sabry@yahoo.com (D.Y. Sabry)*
[b]*Department of Refining, Egyptian Petroleum Research Institute, Cairo, 11727, Egypt, Tel. +201091816259; email: hebachem@yahoo.com*
[c]*Department of Analysis and Evaluation, Egyptian Petroleum Research Institute, Cairo, 11727, Egypt, Tel. +201116560625; email: amr.nada@epri.sci.eg/chem_amr@yahoo.com (A.A. Nada), Tel. +201033055109; email: d_hager80@yahoo.com (H.R. Ali), Tel. +201223631912; email: ymoustafa12@yahoo.com (Y.M. Moustafa)*

Received 1 June 2021; Accepted 7 January 2022

ABSTRACT

Binary composite MoS_2/TiO_2 nanofibers (MTN) were elaborated by electrospinning technique. The photocatalytic efficiency of the binary nanofibers was controlled via different ratios between MoS_2 and TiO_2. The structural, morphology and optical properties of the prepared nanofibers were detected by Raman spectroscopy, Fourier-transform infrared spectra, scanning electron microscopy and UV–Vis diffuse reflectance spectra. The prepared nanofibers were showed remarkable performance in photocatalytic efficiency of phenol compounds degradation under visible light. MTN nanofibers recorded superior photocatalytic activity (96%) and high stability of several cycles under visible light. Therefore, MoS_2/TiO_2 nanofibers have massive implementation prospects for the treatment of wastewater from toxic organic contamination due to their excellent photocatalytic performance reusability and recyclability.

Keywords: Photocatalytic; Molybdenum sulphide; TiO_2; Phenol degradation

1. Introduction

Recently, there are many critical environmental problems in the world, especially water pollution, because of the rapid development of industry [1–3]. Water pollution is a matter of concern worldwide. Wastewater is caused by synthetic chemicals being released from a variety of anthropogenic industry sources. In particular, the petroleum refinery waste which is one of the harmful sources for water, and phenol compound is one of these mischievous sources [3]. The different technologies for water treatment and purification have been extensively discussed in the literature as the design and the operation of affordable methods remains a challenge. The treatment methods include membrane separation, electrochemical method, chemical precipitation, adsorption, photocatalysis, etc. [4–9]. It is pertinent to highlight that all treatment methods have their own technical and economic limitations for real-life applications. However, photocatalysis technique is one of important method as it inhabits the formation of secondary pollutant [6,8]. Titanium dioxide (TiO_2) is one of the most significant photocatalyst, which has been extensively utilized in

* Corresponding author.

Presented at the International Virtual Conference on Water and Energy (ICWE 21), Hassiba Benbouali University of Chlef, Algeria, 25–27 May 2021

various fields, such as electrochemistry and photocatalysis due to its several benefits like low cost, nontoxicity, good chemical stability and excellent oxidizing power [10–12]. However, it has some drawbacks such as lack of activity in the abundant visible light energy due to TiO_2 generally exhibits good photocatalytic activity in near ultraviolet (UV) where it has large bandgap energy (3.2 eV) [6,13,14]. To address these issues, it has been combined with other nanomaterials to enhance its photo-adsorption capacity under visible light such as CdS, NiO, $ZnFe_2O_4$, Ag_2CO_3, Fe_2O_3 and Fe_3O_4 [3,6,8,11,12]. The modification of TiO_2–NFs with substances such as metals, non-metals, semiconductors has been considered to maximize its photocatalytic efficiency [15–18]. The modification of the titanium dioxide has been extensively investigated for environmental purification applications [5], and molybdenum disulphide (MoS_2) is one of the important materials for TiO_2 enhancement.

MoS2 is a typical layered transition metal sulphide with a structure composed of three stacked atom layers (S–Mo–S) [19,20], which has attracted attention due to it has superb stability properties. Also, it has promising photocatalytic applications due to its low band gap [21].

Moreover, there is a synergistic effect of MoS_2 as a 2D support with TiO_2 nanofibers as the 1D structure to improve the active sites, and thus will influence the salient catalytic, electronic and optical properties [16]. In addition, the presence of the sulphur active atoms at the exposed edges of molybdenum disulphide enhances the photocatalytic activity of MoS_2, which has ability to bond with H [22].

In this paper, MoS_2/TiO_2 nanofibers elaborated by combined 1D and 2D structures by electrospinning. The morphology, structure and optical properties of the nanocomposites have been detected. The photocatalytic effect of MoS_2/TiO_2 nanofibers has been estimated under visible light for the degradation of phenol as an organic pollutant.

2. Experimental

2.1. Chemical

Titanium(IV) isopropoxide 97%, MoS_2 powder, n-butyllithium solution, hexane, absolute ethanol (99%), acetic acid (98%), polyvinylpyrrolidone (PVP; Mw = 1,300,000 g/mol), and phenol were purchased from Sigma-Aldrich. All purchased compounds are used as received, without further purification.

2.2. Exfoliation of molybdenum disulphide nanosheets

Molybdenum disulphide was fabricated using the lithium-intercalation-exfoliation method [20]. MoS_2 was stirred in n-butyl lithium solution (1.6 M) for 48 h at 60°C under nitrogen. Furthermore, $LixMoS_2$ was collected and washed several times with hexane, then washed with deionized water and sonicated for 2 h and repeat the washed with deionized water several times until reaching a neutral pH.

2.3. Preparation of MoS_2/TiO_2 nanofibers

Molybdenum disulphide (MoS_2) with TiO_2 nanofibers was prepared using the electrospinning technique by different ratio between MoS_2 and TiO_2. First, the solution (a) was prepared by 0.3 g of PVP dissolved in 3 mL of ethanol and 2 mL of acetic acid while stirring for 30 min, then 1.5 mL of TTIP was added with stirring for 30 min. The solution (b) was prepared with different weight ratios of MoS_2 in 2 mL of ethanol and sonicated for 2 h to get (TM0, TM10, TM20, TM30, TM40 and TM50 for TiO_2:MoS_2 is 1:0, 0.9:0.1, 0.8:0.2, 0.7:0.3, 0.6:0.4 and 0.5:0.5, respectively). After that, solution (b) was mixed to solution (a) with stirring for 30 min. The solution was added in syringe with a stainless-steel nozzle with a diameter of 0.7 mm under flow rate 1 mL/h and voltage power (1.5 kV/cm) between the nozzle and the rotating collector. The collected nanofibers were calcined at 400°C for 3.

2.4. Preparation characterization

The nanofiber structure was detected using the dispersive Raman microscope with a laser wavelength of 532 nm and a power of 10 mW (Senterra, Bruker). The functional groups of the prepared composite nanofibers were recognized using Fourier-transform infrared (FTIR) spectrometer (PerkinElmer) with standard KBr pellets. The Morphology of nanofibers was detected by a scanning electron microscopy (SEM) (Quanta-250 FEG, FEI, The Netherlands). The UV–Vis DR spectra were measured by Jasco V-570.

2.5. Photocatalytic activity measurement

The photocatalytic activity of the MoS_2/TiO_2 nanofibers was detected by photodegradation of phenol. The photocatalyst efficiency was detected by analysing the decrease of phenol concentration during exposure to visible light radiation. The reaction temperature was controlled at 25°C ± 0.2°C by circulating water around the photoreactor. The photocatalytic performance was detected by using 10 mg of photocatalyst in 200 mL of phenol solution (50 ppm) under a 500 W linear halogen lamp (visible light radiation). The solution mixture was stirred in the dark for 1 h to obtain the adsorption/desorption equilibrium of phenol [23]. Then, the mixture was exposed to visible light for 4 h. Then, the sample was collected from reactor every 1 h and the catalyst was eliminated by a centrifuge to detect the organic pollutants concentration in the solution by high-performance liquid chromatography (HPLC) equipped with a photodiode array detector (Agilent 1200 series).

The degradation efficiency was measured by the following equation:

$$\text{Degradation efficiency}\% = \left(\frac{C_0 - C}{C_0}\right) \times 100 \quad (1)$$

where C_0 and C are the initial and final phenol concentration, respectively[24].

The kinetics of phenol photocatalytic degradation was calculated as follows (where, k (min^{-1}) is the apparent rate constant):

$$\ln\left(\frac{C_t}{C_0}\right) = -kt \quad (2)$$

3. Results and discussion

3.1. Materials characterization

The MoS_2/TiO_2 nanofibers with different ratio between molybdenum sulfide and titanium dioxide were detected by Raman. Moreover, Raman spectra of the prepared nanofibers are presented in Fig. 1. The MoS_2 in M sample has peaks at 371 and 403 cm^{-1} which corresponded to E_{12g} and A_{1g} for 2H phase of MoS_2 [21,25,26]. There are also two peaks at 278 and 344 cm^{-1} which are attributed to a small amount of 1T MoS_2 phase [21,26]. In contrast, the T sample has peaks at 147.3, 198.3, 389.2, 501.9 and 626.8 cm^{-1} which corresponded to E_g, E_g, B_{1g}, A_{1g} and E_g modes of TiO_2 anatase phase, respectively [6,8]. The combination of MoS_2 with TiO_2 (in TM10, TM20, TM30 and TM40) resulted in a slight change in the anatase peaks as presented in inset Fig. 1. The TM40 and TM50 had significantly changed the peak at 389 cm^{-1} due to the overlapping between B_{1g} and E_{12g} for TiO_2 and MoS_2, respectively [27]. The conjugation between MoS_2 and TiO_2 can also be detected by the FTIR transmission spectra in Fig. 1b. The band located at around 3512 and 1730 cm^{-1} is attributed to the O–H bond for all nanofibers [13,28]. All nanofibers have a broad band between 650 and 900 cm^{-1} corresponding to the Ti–O bond for TiO_2 [13,28]. There is a band at 605 cm^{-1} in the presence of MoS_2 which correlates to the peak of Mo–S vibration [19,28]. The overlap between the peaks of Ti–O and Mo–S was presented for all nanocomposite sample of TMx which confirmed the successful conjugation between TiO_2 and MoS_2.

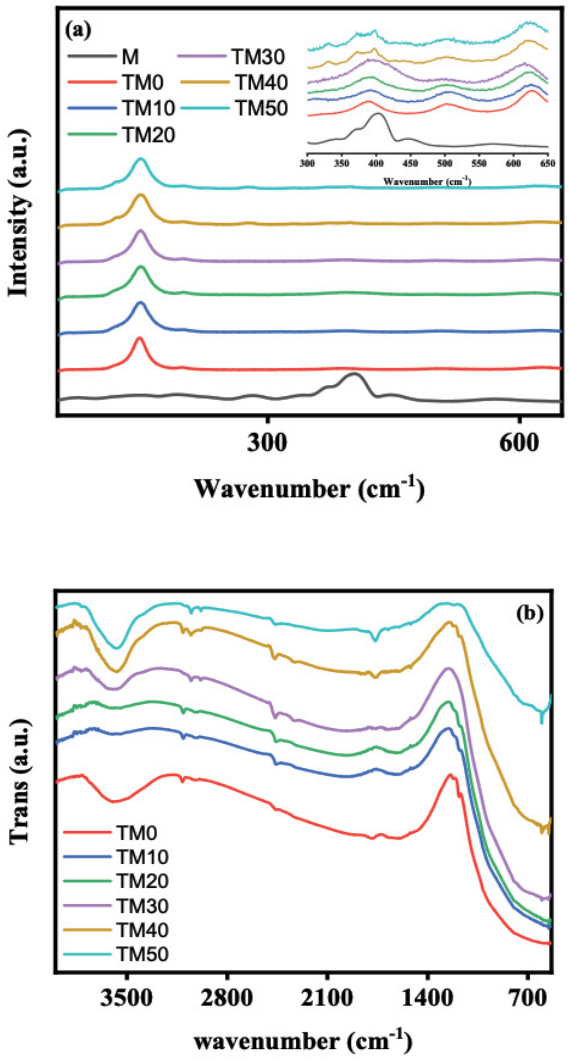

Fig. 1. (a) Raman spectra and (b) FTIR for TM0, TM10, TM20, TM30, TM40 and TM50 nanofibers.

The morphology of fabricated nanofibers was detected using scanning electro microscopy as presented in Fig. 2a–f. The T, TM10, TM20, TM30, TM40 and TM50 nanofibers have 97 ± 8, 116 ± 7, 139 ± 8, 144 ± 5, 159 ± 7 and 183 ± 9 nm average diameter, respectively. The increase in the diameter of the MoS_2-enriched nanofibers was attributed to the viscosity of electrospun solution coming from MoS_2 [29], which contributed to the successful incorporation between MoS_2 and TiO_2 nanofibers [13,29]. These findings are consistent with those of Raman.

The optical phenomena of the fabricated nanofibers were detected using by UV–Vis diffuse reflectance (DR) as presented in Fig. 3. The DR–spectra of the nanofibers were examined in the range of 200–800 nm using UV–Vis optical spectroscopy. The optical band gaps (E_g) were measured from the following equation:

$$\alpha h\nu = A\left(h\nu - E_g\right)^{n/2} \tag{3}$$

where α is the absorption coefficient, υ is the frequency of light, and n is the constant of proportionality (n equal 4 for the indirect transition in the prepared nanofibers).

The prepared nanofibers had a red shift due to joining of MoS_2 with TiO_2 [30]. As per the following sequence: 3.18, 2.66, 2.57, 2.54, 2.46 and 2.43 eV for TM0, TM10, TM20, TM30, TM40 and TM50, respectively. This recorded shift was due to the conjugation between MoS_2 and TiO_2, and this conjugation was also detected in the studies of Raman and FTIR [31]. The TM40 has quenched of intensity more than other nanofibers due to the high absorption of light [12]. In contrast, TM50 had a greater amount of MoS_2, which led to the aggregation of MoS_2 and reduced light absorbed as detected in the SEM image [30].

3.2. Photocatalytic degradation of phenol under visible light by TMx nanofibers

With regard to the photodegradation of phenol, the adsorption equilibrium test in the dark evaluated for 1 h and then photo-catalytic activity for 4 h. The photodegradation of phenol reached 13%, 59%, 71%, 83%, 96% and 92% for TM0, TM10, TM20, TM30, TM40 and TM50, respectively as presented in Fig. 4a. The TM0 for TiO_2 nanofibers recorded lower photodegradation activity of phenol ~ 13% due to the large band gap of TM0 at 3.18 eV. In contrast, the presence of MoS_2 with TiO_2 enhanced the catalytic activity of phenol degradation reaching 96% for TM40. This can be attributed to the reduced band gap leading to activity under visible light as recorded in UV–Vis diffuse reflectance. In addition, the photocatalytic active sites were increased by the incorporation of 1D MoS_2 with 2D TiO_2 nanofibers.

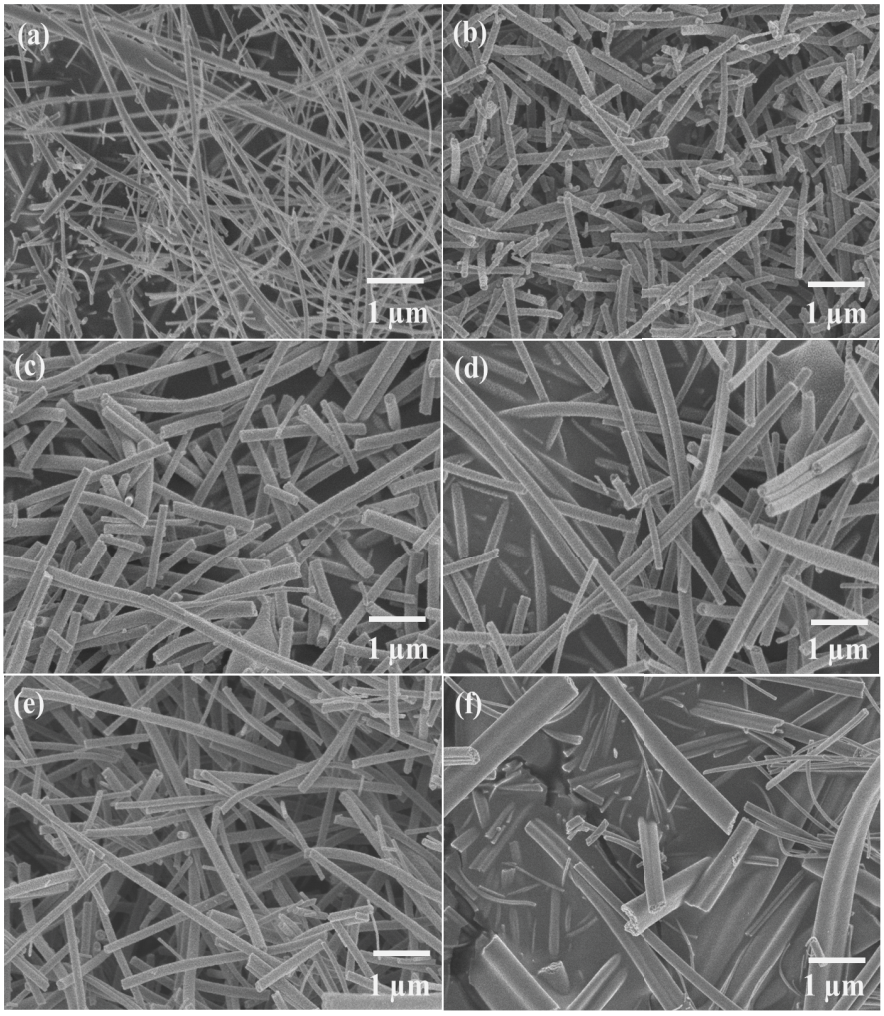

Fig. 2. SEM images for (a) TM0, (b) TM10, (c) TM20, (d) TM30, (e) TM40 and (f) TM50 nanofibers.

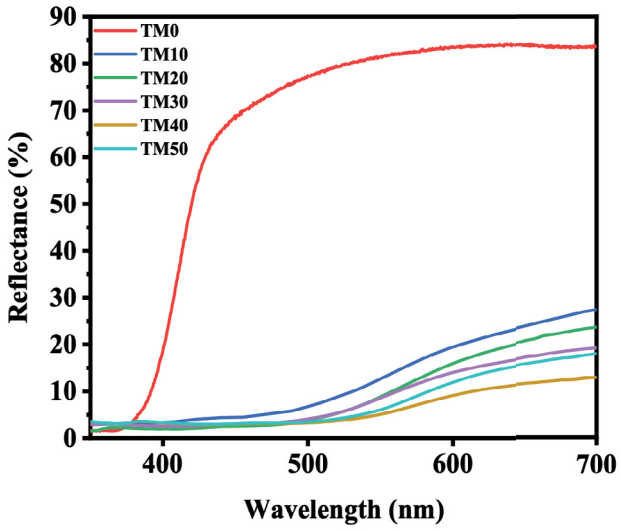

Fig. 3. UV–Vis diffuse reflectance spectra of TM0, TM10, TM20, TM30, TM40 and TM50 nanofibers.

The photodegradation kinetic of phenol by the prepared nanofibers is presented in Fig. 4b. Phenol degradation follows the first-order kinetics model of Langmuir–Hinshelwood which is presented in Eq. (2) [32]. The apparent order rate constant (k) for TM0, TM10, TM20, TM30, TM40 and TM50 is 2.235E-4, 0.002, 0.004, 0.006, 0.012 and 0.007 min^{-1}, respectively. Rate constants grow in this order; TM40 > TM50 > TM30 > TM20 > TM10 > TM0. TM40 records the maximum rate constant (0.012), which was attributed to the high incorporation between MoS_2 and TiO_2 as presented in SEM and Raman and the presence of the synergistic effect between MoS_2 and TiO_2 nanofibers. In order to conclude the role of hydroxyl radicals ($^{\bullet}OH$), holes (h^+) and superoxide anions ($^{\bullet}O_2^-$) in the efficiency of photodegradation of phenol, we used different free radical trapping agents with TM40 nanofibers as presented in Fig. 4c. The scavengers were tert-butyl alcohol (TBA), disodium ethylenediaminetetraacetic acid (Na_2-EDTA) p-benzoquinone (BQ) to trap free radicals of hydroxyl radicals ($^{\bullet}OH$), holes (h^+) and superoxide radicals ($^{\bullet}O_2^-$), respectively [27]. The photodegradation of phenol varied according to different sacrificial agents. Predominantly, the photocatalytic

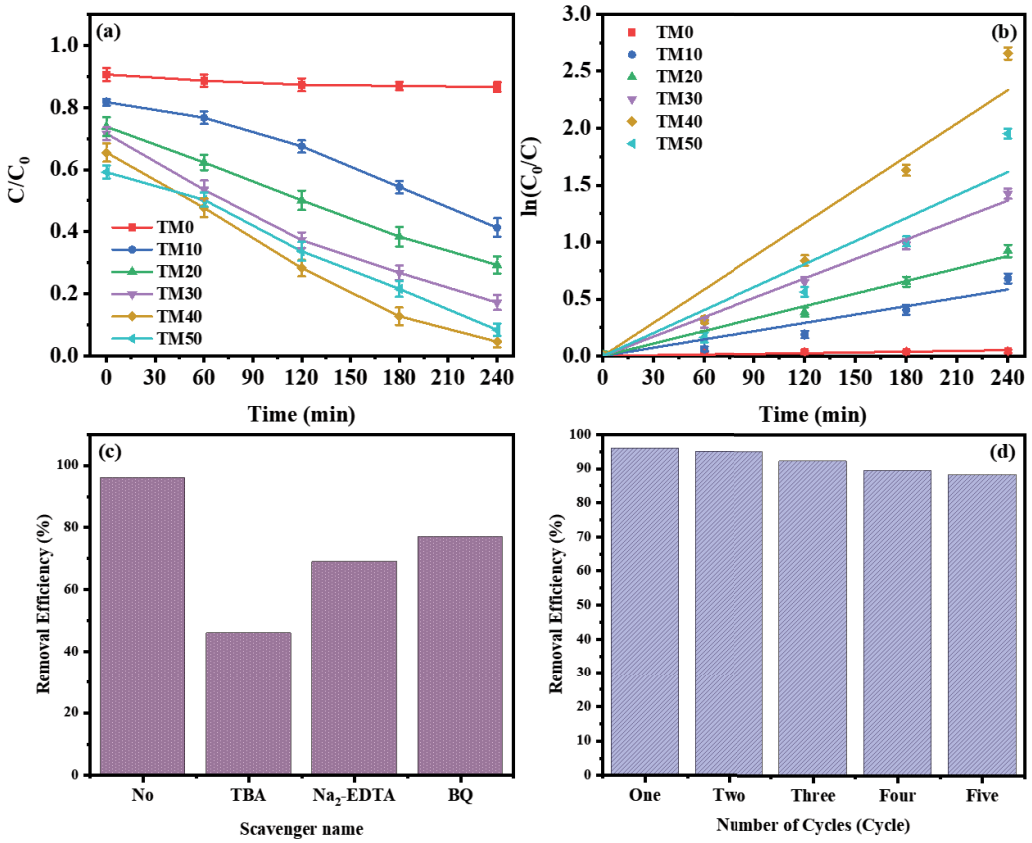

Fig. 4. (a) Photocatalytic degradation of phenol for prepared nanofibers under visible light irradiation, (b) the $\ln(C/C_0)$ changing vs. time during visible light irradiation for prepared nanofibers, (c) trapping test of the photogenerated free radicals and holes with TM40 nanofibers and (d) stability cycles of phenol photodegradation using TM40 nanofibers under visible light irradiation for 4 h.

degradation in presence of the TBA (5 mM) reduced to 46%. Therefore, the •OH radical photogenerated was the important component of free radical during the phenol photodegradation process [33]. Moreover, the TM40 has high photodegradation stability up to five cycles as presented in Fig. 4d. The photodegradation of phenol remained stable at 88.2% after 5 cycles. These TM40 results indicate a high photocatalytic degradation of phenol with a narrow bandgap as well as an excellent stability of photocatalytic activity.

4. Conclusion

In brief, we have successfully prepared MoS_2/TiO_2 nanofibers with different ratios between MoS_2 and TiO_2 (1D and 2D), respectively. Structural and morphological analyses of the prepared nanofibers confirmed the incorporation between MoS_2 and TiO_2. Significantly, the photocatalytic efficiency of TM40 for phenol degradation was as high as 96%. The remarkable photocatalytic performance of TM40 (1D/2D structure) was attributed to the small amount of (1T) MoS_2 acting as a co-catalyst between 2H MoS_2 and TiO_2 to improve electron transfer. In addition, the synergistic effect between MoS_2 and TiO_2 enhanced the photocatalytic stability of the nanofibers. The trapping test for the photogenerated free radicals and holes of TM40 demonstrated that the hydroxyl radicals photogenerated (•OH) has a significant role in the photodegradation of phenol as an organic pollutant. Therefore, MoS_2/TiO_2 nanofibers act as promising materials for photodegradation of organic pollutants in water.

References

[1] M. Najem, A.A. Nada, M. Weber, S. Sayegh, A. Razzouk, C. Salameh, C. Eid, M. Bechelany, Palladium/carbon nanofibers by combining atomic layer deposition and electrospinning for organic pollutant degradation, Materials (Basel), 13 (2020) 1947, doi: 10.3390/ma13081947.
[2] M. El-Sayed, A.A. Nada, Polyethylenimine–functionalized amorphous carbon fabricated from oil palm leaves as a novel adsorbent for Cr(VI) and Pb(II) from aqueous solution, J. Water Process Eng., 16 (2017) 296–308.
[3] H.H. El-Maghrabi, A.A. Al-Kahlawy, A.A. Nada, T. Zaki, Photocorrosion resistant Ag_2CO_3@Fe_2O_3/TiO_2-NT nanocomposite for efficient visible light photocatalytic degradation activities, J. Hazard. Mater., 360 (2018) 250–256.
[4] G.A.M. Ali, A. Barhoum, V.K. Gupta, A.A. Nada, H.H. El-Maghrabi, R. Kanthasamy, E.R. Shaaban, H. Algarni, K.F. Chong, High surface area mesoporous silica for hydrogen sulfide effective removal, Curr. Nanosci., 16 (2020) 226–234.
[5] A.A. Nada, M.F. Bekheet, S. Roualdes, A. Gurlo, A. Ayral, Functionalization of MCM-41 with titanium oxynitride deposited via PECVD for enhanced removal of methylene blue, J. Mol. Liq., 274 (2019) 505–515.
[6] A.A. Nada, H.R. Tantawy, M.A. Elsayed, M. Bechelany, M.E. Elmowafy, Elaboration of nano titania-magnetic reduced graphene oxide for degradation of tartrazine dye in aqueous solution, Solid State Sci., 78 (2018) 116–125.

[7] H.H. El-Maghrabi, S.M. Abdelmaged, A.A. Nada, F. Zahran, S.A. El-Wahab, D. Yahea, G.M. Hussein, M.S. Atrees, Magnetic graphene based nanocomposite for uranium scavenging, J. Hazard. Mater., 322 (2017) 370–379.
[8] A.A. Nada, M. Nasr, R. Viter, P. Miele, S. Roualdes, M. Bechelany, Mesoporous $ZnFe_2O_4$@TiO_2 nanofibers prepared by electrospinning coupled to PECVD as highly performing photocatalytic materials, J. Phys. Chem. C, 121 (2017) 24669–24677.
[9] B. Pant, G.P. Ojha, Y.-S. Kuk, O.H. Kwon, Y.W. Park, M. Park, Synthesis and characterization of ZnO-TiO_2/carbon fiber composite with enhanced photocatalytic properties, Nanomaterials, 10 (2020) 1960, doi: 10.3390/nano10101960.
[10] M.A. Deyab, A.A. Nada, A. Hamdy, Comparative study on the corrosion and mechanical properties of nano-composite coatings incorporated with TiO_2 nano-particles, TiO_2 nano-tubes, and ZnO nano-flowers, Prog. Org. Coat., 105 (2017) 245–251.
[11] H.H. El-Maghrabi, A. Barhoum, A.A. Nada, Y.M. Moustafa, S. Mikhail Seliman, A.M. Youssef, M. Bechelany, Synthesis of mesoporous core-shell CdS@TiO_2 (0D and 1D) photocatalysts for solar-driven hydrogen fuel production, J. Photochem. Photobiol., A, 351 (2018) 261–270.
[12] K.R. Diab, H.H. El-Maghrabi, A.A. Nada, A.M. Youssef, A. Hamdy, S. Roualdes, S. Abd El-Wahab, Facile fabrication of $NiTiO_3$/graphene nanocomposites for photocatalytic hydrogen generation, J. Photochem. Photobiol., A, 365 (2018) 86–93.
[13] A.A. Nada, M.F. Bekheet, R. Viter, P. Miele, S. Roualdes, M. Bechelany, BN/$Gd_xTi_{(1-x)}O_{(4-x)/2}$ nanofibers for enhanced photocatalytic hydrogen production under visible light, Appl. Catal., B, 251 (2019) 76–86.
[14] A.A. Nada, W.M.A. El Rouby, M.F. Bekheet, M. Antuch, M. Weber, P. Miele, R. Viter, S. Roualdes, P. Millet, M. Bechelany, Highly textured boron/nitrogen co-doped TiO_2 with honeycomb structure showing enhanced visible-light photoelectrocatalytic activity, Appl. Surf. Sci., 505 (2019) 144419, doi: 10.1016/j.apsusc.2019.144419.
[15] M.A. Draz, H.H. El-Maghrabi, F.S. Soliman, H. Selim, A.A. Razik, A.E.S. Amin, Y.M. Moustafa, A. Hamdy, A.A. Nada, Large scale hybrid magnetic ZnFe2O4/TiO2 nanocomposite with highly photocatalytic activity for water splitting, J. Nanopart. Res., 23 (2021) 1–10, doi: 10.1007/s11051-020-05122-z.
[16] S. Sayegh, F. Tanos, A. Nada, G. Lesage, F. Zaviska, E. Petit, V. Rouessac, I. Iatsunskyi, E. Coy, R. Viter, D. Damberga, M. Weber, A. Razzouk, J. Stephan, M. Bechelany, Tunable TiO_2-BN-Pd nanofibers by combining electrospinning and atomic layer deposition to enhance photodegradation of acetaminophen, Dalton Trans., 51 (2022) 2674–2695.
[17] S. Kawrani, M. Boulos, M.F. Bekheet, R. Viter, A.A. Nada, W. Riedel, S. Roualdes, D. Cornu, M. Bechelany, Segregation of copper oxide on calcium copper titanate surface induced by Graphene Oxide for Water splitting applications, Appl. Surf. Sci., 516 (2020) 146051, doi: 10.1016/j.apsusc.2020.146051.
[18] S. Kawrani, A.A. Nada, M.F. Bekheet, M. Boulos, R. Viter, S. Roualdes, P. Miele, D. Cornu, M. Bechelany, Enhancement of calcium copper titanium oxide photoelectrochemical performance using boron nitride nanosheets, Chem. Eng. J., 389 (2020) 124326, doi: 10.1016/j.cej.2020.124326.
[19] R. Vinoth, I.M. Patil, A. Pandikumar, B.A. Kakade, N.M. Huang, D.D. Dionysios, B. Neppolian, Synergistically enhanced electrocatalytic performance of an N-doped graphene quantum dot-decorated 3D MoS_2–graphene nanohybrid for oxygen reduction reaction, ACS Omega, 1 (2016) 971–980.
[20] D.M. Sim, H.J. Han, S. Yim, M.-J. Choi, J. Jeon, Y.S. Jung, Long-term stable 2H-MoS_2 dispersion: critical role of solvent for simultaneous phase restoration and surface functionalization of liquid-exfoliated MoS_2, ACS Omega, 2 (2017) 4678–4687.
[21] M.R. Saber, G. Khabiri, A.A. Maarouf, M. Ulbricht, A.S.G. Khalil, A comparative study on the photocatalytic degradation of organic dyes using hybridized 1T/2H, 1T/3R and 2H MoS_2 nano-sheets, RSC Adv., 8 (2018) 26364–26370.
[22] X. Liu, Z. Xing, H. Zhang, W. Wang, Y. Zhang, Z. Li, X. Wu, X. Yu, W. Zhou, Fabrication of 3D mesoporous black TiO_2/MoS_2/TiO_2 nanosheets for visible-light-driven photocatalysis, ChemSusChem, 9 (2016) 1118–1124.
[23] R. Elshypany, H. Selim, K. Zakaria, A.H. Moustafa, S.A. Sadeek, S.I. Sharaa, P. Raynaud, A.A. Nada, Elaboration of Fe_3O_4/ZnO nanocomposite with highly performance photocatalytic activity for degradation methylene blue under visible light irradiation, Environ. Technol. Innovation, 56 (2021) 10458–10476.
[24] S. Sugi, P. Usha Rajalakshmi, J. Shanthi, Photocatalytic degradation efficiency of $Cu_XZn_{1-X}O$ composite, Optik (Stuttg), 131 (2017) 406–413.
[25] U. Gupta, B.S. Naidu, U. Maitra, A. Singh, S.N. Shirodkar, U.V. Waghmare, C.N.R. Rao, Characterization of few-layer 1T-$MoSe_2$ and its superior performance in the visible-light induced hydrogen evolution reaction, APL Mater., 2 (2014), doi: 10.1063/1.4892976.
[26] H. Fan, R. Wu, H. Liu, X. Yang, Y. Sun, C. Chen, Synthesis of metal-phase-assisted 1T@2H-MoS_2 nanosheet-coated black TiO_2 spheres with visible light photocatalytic activities, J. Mater. Sci., 53 (2018) 10302–10312.
[27] H. Fan, R. Wu, H. Liu, X. Yang, Y. Sun, C. Chen, Synthesis of metal-phase-assisted 1T@2H-MoS_2 nanosheet-coated black TiO_2 spheres with visible light photocatalytic activities, J. Mater. Sci., 53 (2018) 10302–10312.
[28] P. Zhou, Y. Shen, S. Zhao, Y. Chen, S. Gao, W. Liu, D. Wei, Hydrothermal synthesis of novel ternary hierarchical MoS_2/TiO_2/clinoptilolite nanocomposites with remarkably enhanced visible light response towards xanthates, Appl. Surf. Sci., 542 (2021) 148578, doi: 10.1016/j.apsusc.2020.148578.
[29] M. Nasr, S. Balme, C. Eid, R. Habchi, P. Miele, M. Bechelany, Enhanced visible-light photocatalytic performance of electrospun rGO/TiO_2 composite nanofibers, J. Phys. Chem. C, 121 (2017) 261–269.
[30] R. Elshypany, H. Selim, K. Zakaria, A.H. Moustafa, S.A. Sadeek, S.I. Sharaa, P. Raynaud, A.A. Nada, Magnetic ZnO crystal nanoparticle growth on reduced graphene oxide for enhanced photocatalytic performance under visible light irradiation, Molecules, 26 (2021) 2269, doi: 10.3390/molecules26082269.
[31] D. Cao, Q. Wang, S. Zhu, X. Zhang, Y. Li, Y. Cui, Z. Xue, S. Gao, Hydrothermal construction of flower-like MoS_2 on TiO_2 NTs for highly efficient environmental remediation and photocatalytic hydrogen evolution, Sep. Purif. Technol., 265 (2021) 118463, doi: 10.1016/j.seppur.2021.118463.
[32] A.S. Morshedy, H.R. Ali, A.A. Nada, A.M. Rabie, H.H. El-Maghrabi, Highly efficient imprinted polymer nanocomposites for photocatalytic desulfurization of real diesel fuel, Environ. Technol. Innov., 21 (2021) 101206, doi: 10.1016/j.eti.2020.101206.
[33] W. Gao, M. Wang, C. Ran, L. Li, Facile one-pot synthesis of MoS_2 quantum dots–graphene–TiO_2 composites for highly enhanced photocatalytic properties, Chem. Commun., 51 (2015) 1709–1712.